

# Intermittent spatio-temporal desynchronization and sequenced synchrony in ECoG signals

Robert Kozma<sup>1,a)</sup> and Walter J. Freeman<sup>2,b)</sup>

<sup>1</sup>Computational NeuroDynamics Laboratory, University of Memphis, Memphis, Tennessee 38120, USA

<sup>2</sup>Division of Neurobiology, University of California at Berkeley, Berkeley, California 94720, USA

(Received 29 February 2008; accepted 18 August 2008; published online 22 September 2008)

Electrocorticographic (ECoG) signals from the brain surface typically exhibit high synchrony across large cortical areas, interrupted by brief periods of desynchronization exhibiting propagating phase discontinuities, across which spatial patterns of phase emerge in selected frequency bands. Experiments with rabbits trained using classical conditioning paradigms indicated that such desynchronization periods demarcate cognitive processing in the subjects; the ECoG in the frames between such periods revealed spatial patterns of amplitude modulation that were classified with respect to sensory stimuli that the rabbits had been trained to recognize. The present work describes intermittent synchrony and desynchronization of ECoG signals measured over the visual cortex. We analyze the analytic amplitude (AA) and analytic phase (AP) of the signals bandpassed over the beta band (12.5–25 Hz) and theta band (3–7 Hz) using the Hilbert transform. The AP of analytic signals evaluated using a Shannon-based synchronization index in theta band exhibits phase synchronization for varying time periods averaging about 1 s, interrupted by desynchronization periods of duration about 0.1 s. Synchronization periods in the beta-band last <100 ms, with interruptions by desynchronization lasting one-tenth that, in which the analytic amplitude drops drastically. During these “null spikes,” the analytic phase is undefined, and the spatial and temporal phase differences show high dispersion. Detailed examination of the bandpass filtered ECoG confirms the presence of a shared mean frequency in a frame of synchronized oscillation, at which frequency the spatial pattern of the AP has the form of a cone. Between frames the AA approaches zero. The form of the null spike resembles a tornado (a vortex), as shown in sequential frames by a rotating spatial pattern of amplitude in the filtered ECoG. © 2008 American Institute of Physics.

[DOI: [10.1063/1.2979694](https://doi.org/10.1063/1.2979694)]

## I. INTRODUCTION

The human brain is prodigious in its consumption of energy. It has 2% of body mass, yet it consumes 20% of metabolic energy at rest and in action.<sup>24</sup> From a macroscopic perspective it is clearly a large-scale thermodynamic system that requires energy for continually adapting to the environment by maintaining itself in a state near criticality.<sup>10</sup> It adapts by repeated discrete steps that are enabled by criticality and revealed at the mesoscopic ECoG level in sequences of spatial patterns of amplitude modulation<sup>6</sup> and phase modulation<sup>12</sup> in ECoG oscillations. The patterns manifest mesoscopic order parameters that organize the microscopic activities of neural masses. Mutual excitation among neurons in positive feedback loops maintains the steady-state “spontaneous” brain activity. Inhibitory neurons enable brain wave oscillations by negative feedback loops. The distributions of feedback delay times give distributions of frequencies. Narrowband oscillations in the theta, alpha, beta, and gamma bands<sup>14</sup> are similar when scaled appropriately in time seg-

ments, revealing self-similarity in the rest state. The oscillations and spectral peaks are selectively enhanced in the theta, beta, and gamma ranges during intentional action. Both at rest and during action, the distributed oscillations in each pass band interfere and form brain waves, so that “beats” appear as a type of Rayleigh noise.<sup>8</sup> The beats have the form of null spikes at which mesoscopic amplitudes cancel, the order parameter vanishes, and the microscopic activity becomes disordered. These sequenced lapses in order provide the degree of freedom brains need for rapid and repeated transitions to new patterns of ordered activity. In our thermodynamic model of the brain, we model these jumps as phase transitions between the ordered and disordered states.<sup>9</sup> This model describes a null spike as the temporal aspect of a vortex of a phase transition in a disordered state, and a phase cone as the spatial aspect that persists into and through an ordered state.

Brains are dynamical systems with trajectories evolving through high-dimensional attractor landscapes that are determined by the subject’s previous experiences, its present state, and its intended future goals. The brain state space is essentially infinite, owing to the complexities of the environment, of individual experiences, and of the brain itself. A finite brain state space can be defined as a projection by a set of measurements of multichannel brain electrical activity simul-

<sup>a)</sup>Present address: Department of Mathematical Sciences, The University of Memphis, 373 Dunn Hall, Memphis, TN 38152, USA. Telephone: 1-901-678-2497. Fax: 1-901-678-2480. Electronic mail: rkozma@memphis.edu. URL: <http://cnd.memphis.edu>.

<sup>b)</sup>Electronic mail: [dfreeman@berkeley.edu](mailto:dfreeman@berkeley.edu).

taneously with conditioned responses to conditioned stimuli. The ECoG data sets derived from  $8 \times 8$  arrays of electrodes on the surface of the cerebral cortex give spatial maps of the amplitude and rate of change of brain activity in the form of a time-varying vector in 64-space.<sup>5</sup> The tip of this vector gives a trajectory in that finite space that displays pauses in circumscribed volumes, when the subject is presented a conditioned stimulus. The location of that volume defines an attractor in 64-space. A collection of attractors forms with a collection of conditioned stimuli, giving a convoluted attractor landscape. There are multiple landscapes coexisting in sensory cortices, each with its frequency pass band. The dwell time in a pause at a given attractor is dependent on the pass band. The transit time between pauses is about one-tenth of the dwell time duration. These results are related to Kelso's metastability concept that has been introduced based on decades-long studies into the coordination dynamics of the brain.<sup>16</sup>

During the pauses, the ECoG displays high synchrony at a relatively constant frequency at which the spatial patterns of phase and amplitude can be defined in a frame. The AA pattern is classifiable with respect to conditioned stimuli. The AP pattern has the geometric form of a cone with a fixed spatial phase gradient in rad/mm corresponding to conduction velocities of intracortical axons in m/s at each frequency in Hz.<sup>11</sup> The ECoG during transitions between frames is strongly desynchronized. Assay of the distinction requires an index of synchrony by any of several methods giving the same results. These include Fourier decomposition of the signals<sup>12</sup> and calculation of phase dispersion, calculation of the ratio of the temporal standard deviation of the mean wave form to the mean SD of the 64 wave forms in a moving window twice the length of the center wavelength of the pass band,<sup>4</sup> an index derived from Shannonian information theory,<sup>13,21,22</sup> and most simply by the spatial standard deviation of the 64 values of analytic phase differences (referred to the preceding values in time in rad), which when divided by the duration of the digitizing step in s give the analytic frequency in rad/s.

The present work studies the intermittent desynchronization and resynchronization demarcated by "null spikes" at which mesoscopic amplitudes cancel by interference. Preliminary results on theta-band EEG phase synchronization analysis were reported in Ref. 25. Here we study theta- and beta-band synchronization. We infer that the order parameter vanishes and the microscopic activity is disordered at the "null spikes." We propose that these sequenced lapses in order provide the degree of freedom brains need for rapid and repeated transitions at criticality to new spatial amplitude patterns of ordered mesoscopic activity.<sup>7,9,10</sup> In our thermodynamic view, we model these jumps as phase transitions between the ordered and disordered states. The delays that are caused by axonal and dendritic propagations impose the observed variation in rates of change in phase, both temporal in rad/s and spatial in rad/mm.<sup>4</sup> These two kinds of phase differences appear as vortices, which are commonly seen as metastable structures resembling tornadoes in close association with phase transitions.<sup>9</sup> Here we describe a null spike as the temporal aspect of a vortex of a phase transition in a

disordered state, and a phase cone as the spatial aspect that appears in disorder and persists through an ordered state.

## II. DETECTING SYNCHRONY IN NETWORKS OF OSCILLATORS

### A. Shannon synchronization index

The synchronization between random variables  $x_n$  and  $x_m$  is measured by calculating the phase coupling based on the Shannon entropy of the phase differences.<sup>21,22</sup> Let  $p_{nm}(k)$  denote the relative frequency of the  $k$ th bin in the histogram of the relative phase  $\varphi_{n,m}$  between the two signals. The Shannon entropy index  $\rho_{n,m}$  is computed as follows:

$$\rho_{n,m} = 1 + \frac{\sum_{k=1}^N p_{n,m}(k) \ln p_{n,m}(k)}{\ln N}, \quad (1)$$

where  $N$  is the number of bins in the histogram. Clearly,  $\rho_{n,m}=0$  corresponds to a uniform distribution and  $\rho_{n,m}=1$  corresponds to unit distribution.

### B. Calculating the analytic signal

In order to evaluate the Shannon synchronization index, one needs to calculate the phases of each signal. Various approaches exist to estimate the phases.<sup>22</sup> We consider the method based in the construction of the complex analytical signal  $z(t)$  (Refs. 2 and 19) using the Hilbert transform HT. To implement this method, a complex signal  $z(t)$  is constructed, based on the scalar signal  $s(t)$ ,

$$z(t) = s(t) + iH(s(t)) = A(t)e^{i\varphi(t)}, \quad (2)$$

$$A(t) = \sqrt{s^2(t) + H^2(s(t))}, \quad \varphi(t) = \arctan \left[ \frac{H(s(t))}{s(t)} \right],$$

where  $H(s(t))$  is the Hilbert transform of  $s(t)$ . Here  $z(t)$  is a complex function, where  $A(t)$  is the analytic amplitude, and  $\varphi(t)$  is the analytic phase. The Hilbert transform of  $s(t)$  is defined as

$$H(s(t)) = \frac{1}{\pi} \text{PV} \int_{-\infty}^{\infty} \frac{s(\tau)}{t - \tau} d\tau \quad (3)$$

Here PV means that integral is taken in the sense of the Cauchy Principal value. Details of the analytic signal evaluation using Hilbert transform can be found in Refs. 2, 26, and 27. Phase  $\varphi(t)$  and amplitude  $A(t)$  have clear physical interpretation only for relatively narrowband signals.<sup>15</sup> Complex, multicomponent signals, including chaos, are abundant in nature.<sup>3</sup> ECoG is a typical example of a complex system with multicomponent effects, and these signals should be decomposed into multiple monocomponent oscillatory parts before Hilbert analysis. The determination of  $\varphi(t)$  is very sensitive to low-frequency trends, and it is difficult to compute the phase of a signal where the null-crossing in the phase space is not well defined.<sup>22</sup>

### C. Signal decomposition using bandpass filters

Bandpassed signals can be readily calculated using the Fourier decomposition method. Two types of filters are

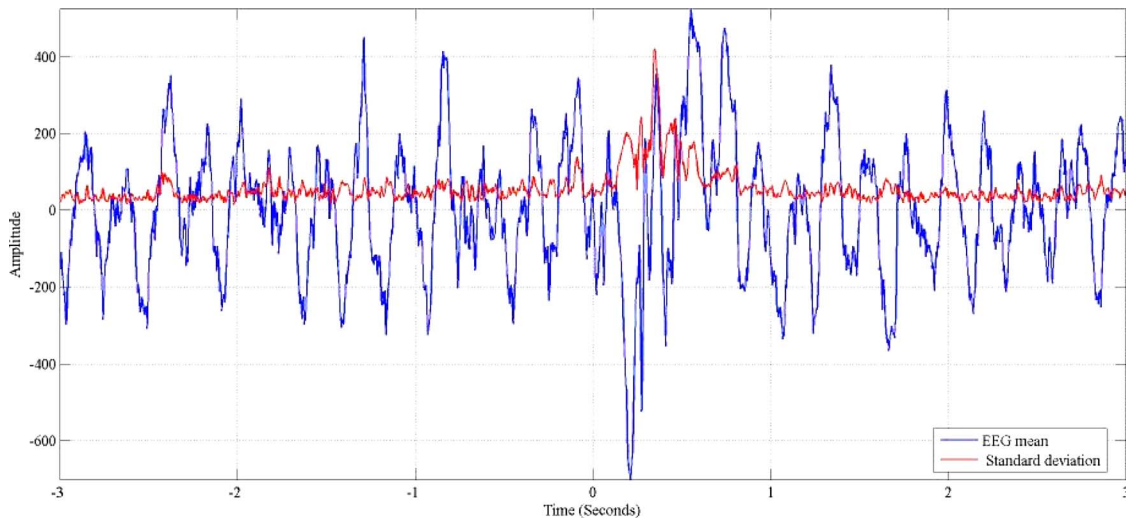


FIG. 1. (Color online) Temporal evolution of the mean and standard deviation of the signals over the 64-electrode array. The increase in mean and SD of the oscillations is clearly seen following the stimulus at the initiation point, 0 s.

readily available for applications, namely infinite impulse response (IIR) and finite impulse response (FIR) filters. IIR filters change the phase of the input while FIR filters do not. In this work, we study phase synchronization effects, therefore we use FIR filters to assure undisturbed phase characteristics.<sup>20</sup> In the data preprocessing phase, we use FIR filters to decompose the complex signals into single-component signals oscillating in a narrow frequency band. In the design of FIR filters, we have to assure reasonable frequency characteristics, i.e., low attenuation in the pass band and high attenuation in the stop band. Since the frequencies are defined by the specific ECoG application, the remaining parameter is the order ( $N$ ) of the FIR filter. We use the least-squares linear phase FIR filters<sup>23</sup> with proper selection of order  $N$ , which assures that the filters reduce the energy around a dominant, while maintaining high energy in the pass band.

### III. DESCRIPTION OF MULTICHANNEL ECoG EXPERIMENTS

#### A. ECoG recordings in rabbits

The electrical activity of the primary visual cortex in rabbits was measured using an  $8 \times 8$  array of electrodes.<sup>1</sup> The space between the electrodes is 0.79 mm covering an area of  $5.6 \text{ mm} \times 5.6 \text{ mm}$ . Data were collected during 6 s using a 500 Hz sampling frequency. During data recording, the signals were low-pass filtered at 100 Hz. 12 bits were used in the quantification process. Experiments have been conducted for duration of 6 s, which have been divided into 3 s pre-stimulus and 3 s poststimulus periods, respectively. This gave a total of 3000 sample points for each of the 64 channels. The rabbits were trained to discriminate visual conditioned stimuli eliciting conditioned responses.<sup>11,12</sup> Figure 1 shows the mean and spatial standard deviation of the 64 signals over the  $8 \times 8$  electrode array.

Initial results of the analysis over the theta band have been reported in Ref. 25. Here the basics of the signal processing methods are outlined, followed by the interpretation

of the obtained results in terms of spatio-temporal dynamic pattern formation. We decompose each signal in the  $8 \times 8$  array of electrodes using FIR filters. We focus in the theta band. To detect the peaks in the frequency domain, we compute the discrete Fourier transform (based in the fast Fourier transform) using the Welch method.<sup>29</sup> We apply a Hamming window of length 512 with 50% overlap. The peak frequency is determined as the frequency having the largest spectral value in the range 3–7 Hz for the theta oscillations. Theta oscillations are extracted by using a bandpass filter with cut-off frequencies of  $5 \text{ Hz} \pm 2 \text{ Hz}$ . The order of the filter  $N$  is set to 181 and the attenuation in the pass band and stop band are 1 and 40 dB, respectively. We use the *firls* Matlab function, which implements least-squares FIR filters.<sup>25</sup>

#### B. Computing the analytic signal

The analytic signal has been calculated for each ECoG channel after filtering in the theta band. Figure 2 illustrates the result in the theta band for two channels. Figure 2, first column, shows from top to bottom (a) the signal of the first channel as a function of time, (c) the real and the imaginary part of the analytical signal, (e) the phase of the signal, and (g) the polar plot in the phase space, respectively. The second column shows the same quantities for the second channel. To reduce boundary effects, 0.5 s of data has been eliminated at the beginning and ending of each signal. We are especially interested in the phase of the analytic signals, the third diagrams from top in both columns. The phase has a typical monotonously increasing tendency from  $-\pi$  to  $+\pi$  for some time segments, interrupted by a discontinuity when it reaches  $+\pi$ . This is due to the circular frequency calculation according to  $\text{mod } 2\pi$ . There are some exceptions from the general monotonous increasing tendency, as seen at around  $-1.5 \text{ s}$  in the second signal. The reason for this effect is discussed in the next section.

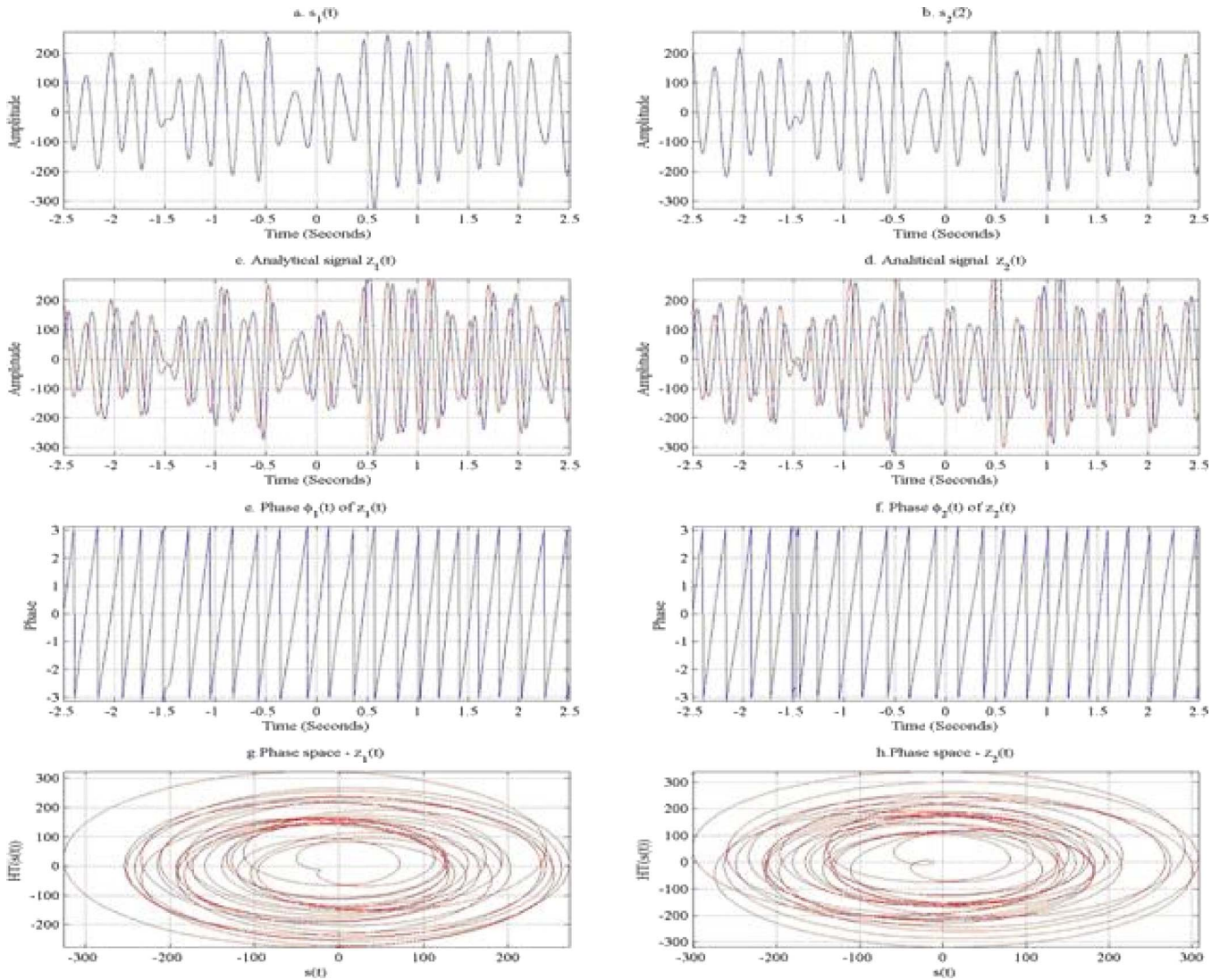


FIG. 2. (Color online) Computing the analytic signal via Hilbert transform. (a) Signal  $s_1(t)$ . (b) Signal  $s_2(t)$ . (c) Analytical signal  $z_1(t)$ . (d) Analytical signal  $z_2(t)$ . (e) Instantaneous phase  $\phi_1(t)$ . (f) Instantaneous phase  $\phi_2(t)$ . (g) Phase space for  $z_1$  and (h) phase space for  $z_2(t)$ .

**C. Phase unwrapping**

In order to track the behavior of the phase over time, the discontinuous phases are straightened by adding  $2\pi$  at the points of discontinuity, to get the unwrapped analytical phase. The slope of the unwrapped phases gives the frequency over time. Oscillations in the slope reflect variations in the frequency content of theta oscillations.<sup>8</sup> Figure 3, upper panel, shows the original phase values, while the lower plot shows the unwrapped phases for all of the 64 signals.

Figure 3 shows that the unwrapped phases contain regions of near-linear behavior, as well as regions of upward and downward deviations from the mean phase. Note that the significant deviations from constant slope happen at some well-defined times for all channels, e.g., at around 1.6, 2.8, and 3.8 s. The slope of the phase curve gives the instantaneous frequency  $f(t)$ . A first-order approximation of the instantaneous frequency for each variable is calculated as follows:

$$f(t) = \frac{1}{2\pi} \frac{d\varphi(t)}{dt} \approx \frac{1}{2\pi} \frac{\Delta\varphi(t)}{\Delta t} = \frac{1}{2\pi} \frac{\varphi(t) - \varphi(t - \Delta t)}{\Delta t}. \quad (4)$$

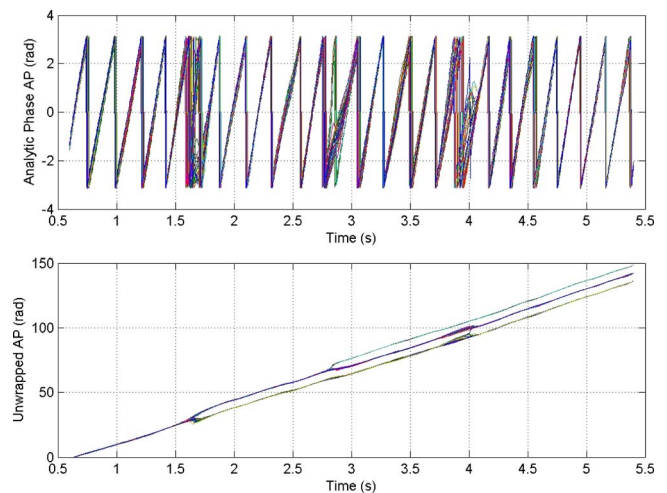


FIG. 3. (Color online) Circular and unwrapped phases for the 64 channels. Observe periods of synchronization and desynchronization. The pitchfork split in the unwrapped phase results from leakage of low-frequency power into the pass band on some channels but not others, owing to the spatial variations in amplitude of all frequency components. Hence some signals will have  $\pi$  radians added with zero crossings, but others will not, owing to failed or extra zero crossings occasioned by the leakage of low- or high-frequency power into the pass band in null spikes.

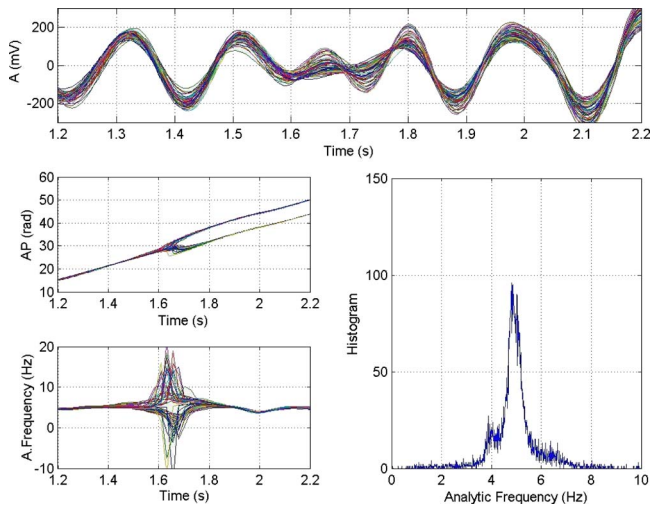


FIG. 4. (Color online) Illustration of various synchronization segments in the theta band. Top panel: 64 channels in time; left-middle: unwrapped phases; left-bottom: analytic frequencies; right-bottom: the distribution of analytic frequencies.

## IV. ANALYSIS OF SYNCHRONIZATION AND DESYNCHRONIZATION EVENTS

### A. Instances of synchronous cortical oscillations

As shown in Fig. 3, there are extended segments with well-defined phase synchronization and shorter segments where the synchronization apparently diminishes. Now we study in detail various segments of the multichannel data to identify different synchronization states. In Fig. 4, during time segments 1.2–1.5 and 1.8–2.2 s, we observe nice phase synchronization with analytic frequency peaking at around 4.5 Hz.

In the top part of Fig. 4, the amplitude of the signals in the mesoscopic array is shown. Figure 4, left-middle diagram, shows the unwrapped phase, while the left-bottom panel depicts the analytic frequency for the 64 channels. The frequencies have been smoothed using a fourth-order moving average filter. Except for the time interval 1.5–1.8 s, the unwrapped phases look like straight lines, resembling sine-like waves with a well defined oscillation peak. Observe that the signals oscillate in the narrowband of frequencies around 4.5 Hz, with the exception of the 1.5–1.8 s segment, where the frequencies exhibit large dispersion over a broad range. In the next section, it is shown that such a dispersion of the frequencies is the indication of the imminent onset of desynchronization.

In order to calculate the Shannon synchronization index, we evaluate the relative phase between various signals. We calculate the phase difference between neighboring channels as follows. The phase of channel  $j$  ( $j=1, \dots, 56$ ) has been subtracted from channels  $k=j+8$ , which gives the phase difference between neighboring channels from consecutive rows of electrodes. The distribution of the phase differences peaks at zero, indicating that phases of the channels in the mesoscopic array strongly synchronize at this time segment. The Shannon synchronization index is 0.90. This dynamics corresponds to absolute phase synchronization,<sup>17</sup> and it indicates the tendency of the units of a coupled system to move

together. This dynamics is also known as “classical phase synchronization.”<sup>22</sup> In classical phase synchronization, the components of the system adjust their phases as a result of weak interaction. Classical phase synchronization is considered a central mechanism for neuronal information processing.<sup>22</sup>

### B. Relative phase synchronization in cortical oscillations

Figure 4 shows phase desynchronization from 1.5 to 1.8 s. Desynchronization is due to the fact that some channels apparently oscillate faster than others. As discussed in the previous section, before 1.5 s and after 1.8 s the channels agree in amplitude and phase. The unwrapped phases in Fig. 4 (middle-left) show that the channels start to desynchronize at around 1.5 s. The desynchronization period takes about 0.2 s. When comparing the distribution of the analytic frequencies, we can see that the spread of the frequency histogram is much larger during the segment 1.5–1.8 s. In Fig. 4, right-bottom panel, only the positive frequencies are shown. The Shannon synchronization index is 0.75, which is a significant drop from its previous value (0.9). Such behavior indicates relative phase synchronization.<sup>22</sup> In this case, the distribution of analytic frequencies and the phase differences have a broader range of values, although synchronization is still present as the distributions have a dominant peak.

Relative phase synchronization is different from phase synchronization in the classical sense.<sup>17,22</sup> In classical phase synchronization, all the coupled components of the system perform alike. In relative phase synchronization, the components of the system have increased autonomy and oscillate at a broader range of frequencies around the dominant frequency in the given frequency band. In the ECoG experiments, we observe periods with phase synchronization in the classical sense interrupted by periods with relative phase synchronization in the theta band. In Fig. 4, the analytic frequency plot shows negative values, which have no physical meaning other than a sudden resetting of the phase. They are due to the fact that some of the ECoG channels have analytic signals with trajectories that miss the origin during the drastic drop of the analytic amplitude. This effect, called null spike, is the manifestation of the diminishing analytic amplitude during desynchronization.

In the next section, we analyze the evolution of the desynchronization into resynchronization yielding a specific spatial structure in the analytic phase called phase cones. Phase cones arise and disappear typically at time scales much shorter than the dominant pass band. To describe their effect, the terminology “sequenced synchrony” is proposed. In the next section, characterization of spatio-temporal structures of sequenced synchrony state is given.

## V. DISCUSSION

### A. Spatial distribution of phase during synchronization period

Analysis of various ECoG data clearly confirmed the previously described synchronization and intermittent desynchronization effects. Looking at the trajectory of the analytic

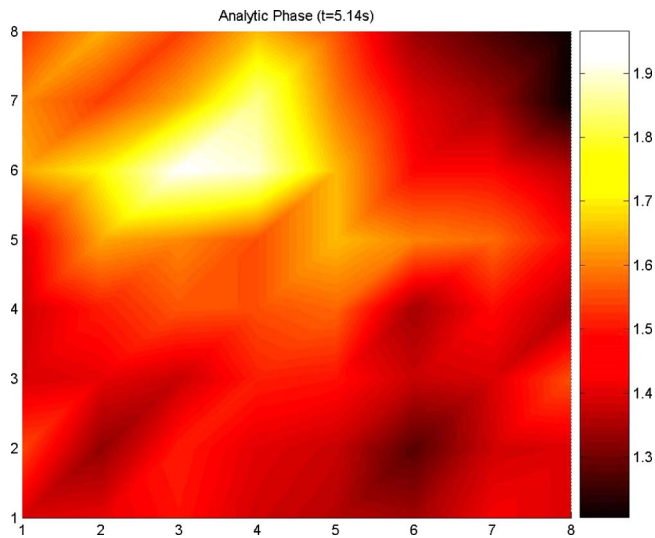


FIG. 5. (Color online) Spatial distribution of analytic phase across the  $8 \times 8$  ECoG electrode array at the time frame  $t=5.14$  s. The phase lags conform with the notion of a phase cone, which is centered toward the upper-left corner of the array.

signals in the complex plane, it is clear that the observed high variances of the analytic phase and desynchronization are due to the fact that the signals approach the origin. This effect is also called null spike,<sup>9</sup> and proper care is needed to identify the physically and physiologically relevant effects, and distinguish them from nonphysical artifacts.

First we analyze the spatial distribution of the analytic phase. During the period of absolute phase synchronization, the phase oscillates at a base level, while previous studies indicated the occurrence of propagation phase gradients in the form of a cone, which are called phase cones.<sup>1,5</sup> Our analysis confirms the presence of phase cones in the theta-band analytic signals. A snapshot of the spatial distribution of the analytic phase is shown in Fig. 5, at time instant  $t = 5.14$  s. The phase distribution is not random; rather it has a clear conical spatial structure, with extreme values of the phase at the apex location, close to the upper left corner of the array in the case of Fig. 5.

The maximum phase difference between the apex of the cone and more remote locations in the array is up to about 0.6 rad, i.e., it approaches  $\pi/4$ . Such characteristic cone patterns appear at various spatial locations and they evolve in space-time by having increasing phase lag values and may cover a significant part of the observation window provided by the  $8 \times 8$  electrode array. This cone existed for about 80 ms, and ultimately disintegrated. The size shown in Fig. 5 is close to the maximum observed. Phase cones persist for time duration, which is typically a fraction of the period determined by the dominant theta oscillation frequency.

### B. Vortices of amplitude oscillations during sequenced synchrony transitions

At the end of the absolute synchronization period, the uncertainty of the analytic phase increases and the analytic amplitude diminishes (null spike). As we approach the desta-

bilization, the analytic amplitude exhibits a peculiar vortex-like pattern, as shown in Fig. 6. Results in Fig. 6 have been obtained by interpolation over the  $8 \times 8$  array using the Matlab surface interp function.

The null spike is the temporal marker for the transition by which a new amplitude modulation pattern forms. The spatial patterns of amplitude modulation (AM) and phase modulation (PM) are established early during a return to high analytic amplitude, as measured by the location of the apex of the cone in PM and the location of the tip of the classificatory feature vector in 64-space, well before the analytic power returns to a maximum. Despite the background noise in which these patterns are immersed, including the multiplicity of overlapping phase cones at differing carrier frequencies, it is often possible to observe clockwise or counterclockwise rotation of filtered ECoG amplitude maxima and minima (not AA) in successive frames (Fig. 6, frames 1–19), as predicted from the static measurements of spatial patterns of analytic phase (AP) at successive points in time giving an invariant phase cone (apex of phase lead at “+” in Fig. 6, frame 20).

The presence of vortices in the cortical amplitude patterns has been predicted based on theoretical arguments.<sup>9,14</sup> Our results show that the synchrony is not completely lost during the transitional period at the null spike; rather it is represented by sequentially appearing semilocalized mesoscopic vortex structures. Thus the described phenomenon is called sequenced synchrony.

Models of spatio-temporal neurodynamics in cortical tissues focusing on phase transitions have been proposed based on graph-theoretical models,<sup>18</sup> and using differential equations with distributed parameters.<sup>17</sup> Intensive research is being conducted at present to interpret these experimental findings, and develop the necessary tools for cognitive monitoring of brain states based on these results.<sup>28</sup>

## VI. CONCLUSIONS AND FUTURE PERSPECTIVES

Synchronization in phase is most likely due to the networks of excitatory neurons that are interconnected by inhibitory synaptic connections. Thus, the recorded ECoG signals do not correspond to individual oscillating neurons. Recorded ECoG signals correspond to the interaction of many coupled neural populations. The computation of the analytical signal via the Hilbert transform allows us to compute the instantaneous phase and the instantaneous energy without assumptions about the linearity and stationarity in the ECoG records. As shown here, this method is quite robust since it is able to capture the analytic phases in signals with well-defined peaks in the power spectrum. Two regions have been identified in the analytic phases: one with a narrow range of analytic frequencies (straight unwrapped phase), and the other with a wide range of frequencies (significant variation in the slope of the phase constituting phase slip). This observation indicates the emergence of various interacting objects, which intermittently can manifest highly individual behaviors or collective oscillations as time evolves.

Such a dual behavior of coupled cortical populations is deemed to be a critical condition to produce the highly com-

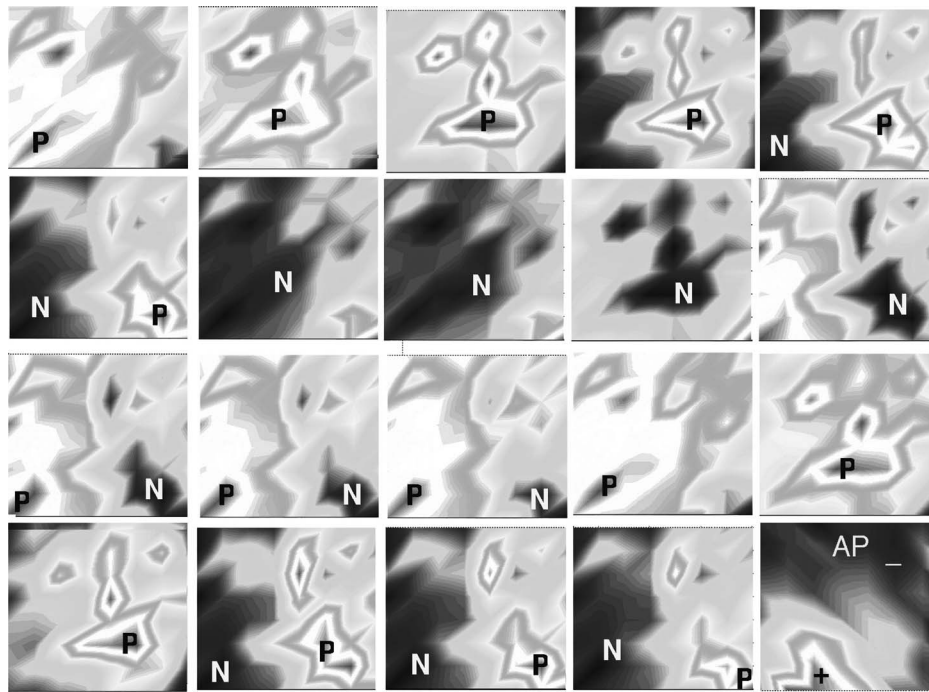


FIG. 6. Temporal evolution of the spatial distribution of amplitudes during the sequenced synchrony state. Each frame shows the spatial pattern of filtered ECoG amplitude (mid-beta range, 20–25 Hz, *P*, positive; *N*, negative; not analytic amplitude, AA, which is non-negative) normalized to within-frame maximum (light) and minimum (dark). The frames are in 4 ms steps, from left to right in one row, and from top to bottom in consecutive rows. One cycle is completed in the first 13 frames (fourth frame in third row), after which the spatial pattern of amplitude repeats. The extremes of positive and negative amplitude move across the frame from left to right indicating clockwise rotation about a point below the lower edge of the frame. The lower right frame labeled “AP” shows the phase cone associated with this sequence of frames with “+” showing phase lead and “-” showing phase lag. This conic pattern formed during a vortex lasting  $\sim 10$  ms and persisted for  $\sim 200$  ms as a stable phase cone. Amplitude patterns rotated either clockwise (as here) or counterclockwise, or most commonly they repeatedly pulsed outwardly (“explosion”) or inwardly (“implosion”) at the carrier frequency.

plex spatio-temporal oscillations that are the hallmarks of higher intelligence and cognition, because it is essential that patterns of neural activity change in accordance with the changing environment. Hence the formation of a new cortical activity pattern in synchronization must be preceded by desynchronization, as the prior pattern disappears and the way is opened for construction and emergence of a new pattern. That transition is marked by the occurrence of a major decrease in analytic amplitude, which appears in the time domain as a null spike and in the spatial domain as a phase cone, which is preserved through the ensuing frame until the next episode of desynchronization.

In this work, we analyzed the evolution of synchronization and desynchronization in Electrocorticograph arrays. Our analysis indicates the sequence of periods with high and low synchrony, as measured by the Shannon synchronization index. It is shown that desynchronization has a specific spatial amplitude structure in the form of phase cones. Phase cones arise and disappear typically at time scales much shorter than the dominant pass band. To describe their effect, the terminology “sequenced synchrony” is proposed.

Further studies are needed to evaluate the detailed spatio-temporal dynamics of such sequenced synchronous states. We propose three experimental tests of our theory of the scalp EEG correlates of perceptual frames at the mesoscopic level.

- We expect that the mesoscopic neural activity in each EEG frame will be continuously distributed over the underlying

cortex as an embedding field for coordinated microscopic activity and not the transient linkage of discrete cortical modules with no phase-locked EEG activity between the linked areas.

- We expect to find textural patterns of amplitude modulation of a shared carrier wave form that can be quantitatively described as feature vectors in  $n$ -space, in which the high and low amplitudes at all points on the scalp within an area of coherence will have classificatory information of equal value for assignment to clusters of points in  $n$ -space, in contrast to a modular hypothesis by which high amplitudes of activity on selected channels can serve to localize discrete cortical modules.
- We predict that the EEG segments of relative constancy of carrier frequency (stationary behavior between null spikes) will have continuously varying phase values constituting phase gradients resembling phase cones in ECoG and not zero-lag phase locking between discrete cortical modules.

We are well aware of the technical difficulties that must be met and solved in order to test the above predictions properly. A detailed description of the proposed way to validate these predictions will be the topic of future studies.

## ACKNOWLEDGMENTS

This work is supported in part by a National Research Council award to R.K. We thank the anonymous reviewers for helpful comments. Contributions by Jose Rodriguez to

the data analysis and to the initial evaluation of the theta-band desynchronization effects are greatly appreciated.

- <sup>1</sup>J. M. Barrie, W. J. Freeman, and M. Lenhart, "Modulation by discriminative training of spatial patterns of gamma EEG amplitude and phase in neocortex of rabbits," *J. Neurophysiol.* **76**, 520–539 (1996).
- <sup>2</sup>B. Boashash, "Estimating and interpreting the instantaneous frequency of a signal. II. Algorithms and applications," *Proc. IEEE* **80**, 540–568 (1992).
- <sup>3</sup>J. Crutchfield, D. Farmer, N. Packard, R. Shaw, G. Jones, and R. Donnelly, "Power spectral analysis of a dynamical system," *Phys. Lett.* **76**, 1–4 (1980).
- <sup>4</sup>W. J. Freeman, "Origin, structure and role of the background EEG activity. Part 1. Analytic amplitude," *J. Clin. Neurophysiol.* **115**, 2077–2088 (2004).
- <sup>5</sup>W. J. Freeman, "Origin, structure and role of the background EEG activity. Part 2. Analytic phase," *J. Clin. Neurophysiol.* **115**, 2089 (2004); **115**, 2107 (2004).
- <sup>6</sup>W. J. Freeman, "Origin, structure, and role of background EEG activity. Part 3. Neural frame classification," *J. Clin. Neurophysiol.* **116**, 1118–1129 (2005).
- <sup>7</sup>W. J. Freeman, "Origin, structure, and role of background EEG activity. Part 4. Neural frame simulation," *J. Clin. Neurophysiol.* **117**, 572–589 (2006).
- <sup>8</sup>W. J. Freeman, "Hilbert transform for brain waves: Entry for Encyclopedia for Computational Neuroscience," in *Scholarpedia*, edited by E. Izhikevich, Vol. 2, Issue 1 (2007), p. 1338 (on-line edition, ISSN 1941-6016), <http://www.scholarpedia.org>.
- <sup>9</sup>W. J. Freeman, "Proposed cortical "shutter" mechanism in cinematographic perception," in *Neurodynamics of Cognition and Consciousness*, edited by L. Perlovsky and R. Kozma (Springer-Verlag, Heidelberg, 2007), pp. 11–38.
- <sup>10</sup>W. J. Freeman, "A pseudo-equilibrium thermodynamic model of information processing in nonlinear brain dynamics," *Neural Networks* **21**, 257–265 (2008).
- <sup>11</sup>W. J. Freeman and B. Baird, "Relation of olfactory EEG to behavior: Spatial analysis: Behavioral," *Neuroscience* **101**, 393–408 (1987).
- <sup>12</sup>W. J. Freeman and J. M. Barrie, "Analysis of spatial patterns of phase in neocortical gamma EEGs in rabbits," *J. Neurophysiol.* **84**, 1266–1278 (2000).
- <sup>13</sup>W. J. Freeman and L. J. Rogers, "Fine temporal resolution of analytic phase reveals episodic synchronization by state transitions in gamma EEG," *J. Neurophysiol.* **87**, 937–945 (2002).
- <sup>14</sup>W. J. Freeman and G. Vitiello, "Dissipation and spontaneous symmetry breaking in brain dynamics," *J. Phys. A: Math. Theor.* **41**, 304042 (2008).
- <sup>15</sup>N. E. Huang, Z. Shen, S. R. Long, M. C. Wu, H. H. Shih, Q. Zheng, N. C. Yen, C. C. Tung, and H. H. Liu, "The empirical mode decomposition and the Hilbert spectrum for nonlinear and nonstationary time series analysis," *Proc. R. Soc. Lond. A* **454**, 903–995 (1998).
- <sup>16</sup>S. Kelso, *Dynamic Patterns: The Self-organization of Brain and Behavior* (MIT Press, Cambridge, MA, 1995).
- <sup>17</sup>R. Kozma and W. J. Freeman, "Chaotic resonance—Methods and applications for robust classification of noisy and variable patterns," *Int. J. Bifurcation Chaos Appl. Sci. Eng.* **11**, 1607–1629 (2001).
- <sup>18</sup>R. Kozma, M. Puljic, B. Bollobas, P. Balister, and W. J. Freeman, "Phase transitions in the neuropercolation model of neural populations with mixed local and non-local interactions," *Biol. Cybern.* **92**, 367–379 (2005).
- <sup>19</sup>J. Marple and S. Lawrance, "Computing the discrete time analytic signal via FFT," *IEEE Trans. Signal Process.* **47**, 2600–2603 (1999).
- <sup>20</sup>A. Oppenheim and W. Schaffer, *Discrete-Time Signal Processing* (Prentice-Hall, Englewood Cliffs, NJ, 1989).
- <sup>21</sup>A. Pikovsky, M. Rosenblum, and J. Kurths, "Phase synchronization in regular and chaotic systems," *Int. J. Bifurcation Chaos Appl. Sci. Eng.* **10**, 2291–2305 (2000).
- <sup>22</sup>A. Pikovsky, M. Rosenblum, and J. Kurths, *Synchronization. A Universal Concept in Nonlinear Sciences* (Cambridge University Press, Cambridge, UK, 2001).
- <sup>23</sup>B. Porat, *A Course in Digital Signal Processing* (Wiley, New York, 1997).
- <sup>24</sup>M. E. Raichle, "The brain's dark energy," *Science* **314**, 1249–1250 (2006).
- <sup>25</sup>J. Rodriguez and R. Kozma, "Phase synchronization in mesoscopic electroencephalogram arrays," *Intelligent Engineering Systems Through Artificial Neural Networks* (ASME Press, New York, 2007), Vol. 17, pp. 9–14.
- <sup>26</sup>A. Pikovsky, M. Rosenblum, and J. Kurths, "Synchronization approach to analysis of biological systems," *Fluct. Noise Lett.* **4**, 53–62 (2004).
- <sup>27</sup>A. Pikovsky, M. Rosenblum, and J. Kurths, "Phase synchronization of chaotic oscillators," *Phys. Rev. Lett.* **76**, 1804 (1996).
- <sup>28</sup>W. Singer and C. Gray, "Visual feature integration and the temporal correlation hypothesis," *Annu. Rev. Neurosci.* **18**, 555–586 (1995).
- <sup>29</sup>P. Welch, "The use of fast Fourier transform for the estimation of power spectra: A method based on time averaging over short, modified periodograms," *IEEE Trans. Audio Electroacoust.* **AU-15**, 70–73 (1967).